model-based clustering function (mclust method),[14,15] which is an R (a free software environment for statistical computing and graphics) package for normal mixture modeling through expectation maximization, model-based clustering, discriminant analysis, and density estimation. The results of ICA with these 3 variables were classified into ≥2 clusters by the mclust method[14,15] to select the most appropriate model for the data (online-only Data Supplement Figure 2). The noise reduction by the wavelet thresholding method (hybrid threshold method),[9,10] the radical ICA, and the mclust method was performed with R software.

i-ICA for Determination of Origin

The i-ICA is an original method developed by 1 of the authors (Y.I.)[11] (online-only Data Supplement) and was applied to the results of ICA to investigate the origin of each T-wave component extracted by ICA (ie, the distribution of each component on the observed surface ECG). Through this analysis, we also confirmed that each IC was a significant T-wave component, not a noise, and thus, the number of ICs could be determined in each case.

Results

Noise Reduction by Wavelet Thresholding Method

Noise reduction (ie, approximation of the data) by wavelet thresholding method could be appropriately applied to all cases and was useful for the following ICA (online-only Data Supplement). Figure 1 shows a typical noise-reduction technique in a normal subject.

ICA and i-ICA in Normal Subjects

The best model was selected from 160 times ICA based on the 3 indices mentioned previously followed by the mclust method. (Details of the selection of the best model by mclust method are provided in the online-only Data Supplement.) Because the number of ICs does not theoretically exceed the number of data (ECG leads), 10 ICs at maximum were obtained by ICA in each case (Figure 2). However, in all 30 normal subjects, the T wave of the best model comprised 4 ICs. Those ICs were arbitrarily called *pre-T*, *early-T*, *middle-T*, and *late-T*, in the order of their appearance. A typical example is presented in Figure 3 and online-only Data Supplement Figure 3. In the next step, we applied i-ICA to the results of ICA in order to recognize the local distribution of each IC on the original ECG (Figure 3). Early-T became the maximum in the vicinity of V3 and V4 and formed the early phase of the T wave. Late-T was the main contributor to the V5 waveform. The middle-T occupied the area between early-T and late-T. Pre-T existed in the early phase of early-T in V3 and V4 (Figure 3, online-only Data Supplement Figure 3), although this IC was not always extracted. When absent, a small positive wave (last-T) instead of pre-T appeared after late-T in V4 to V6, making the number of ICs 4 in all normal subjects.

ICA and i-ICA in LQT1

The number of ICs of the best model that formed the T wave was ≥5 in all 22 patients with LQTS. Five ICs, 6 ICs, and 8 ICs were extracted in 14 patients, 7 patients, and 1 patient, respectively (Table). These ICs comprised the 3 previously mentioned normal ICs (ie, early-T, middle-T, and late-T) and ≥2 additional ICs. We call the latter extra ICs *ExT1*, *ExT2*, and *ExT3*. ICs extracted from the T wave in LQTS are shown

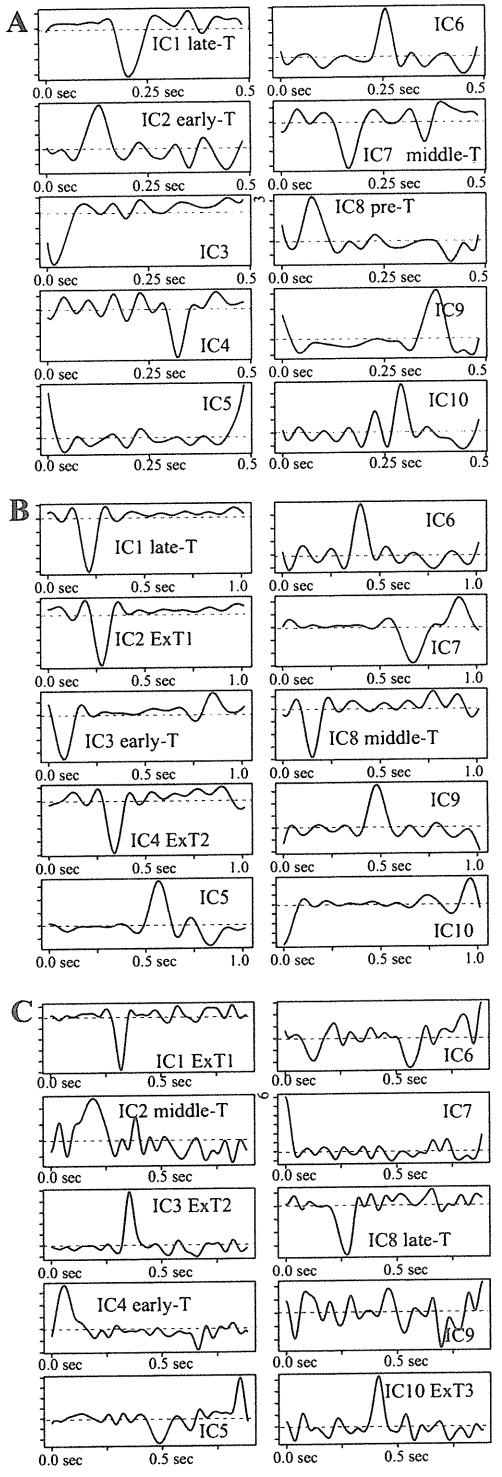

Figure 2. Ten ICs extracted by independent component analysis (ICA) in a normal subject and patients with long-QT syndrome. **A**, Ten ICs of the best model of a typical normal example. The 10 ICs were extracted by the ICA of the second time of the SD 0.7 group among 160 times ICA results. **B**, Ten ICs extracted by ICA, including 2 extra ICs, in a typical example of LQTS with 5 ICs. **C**, Ten ICs extracted by ICA, including 3 extra ICs, in a typical example of LQTS with 6 ICs. IC indicates independent component; ICx, the xth IC that appears in sequence by ICA (x=1 to 10 at maximum because the number of ICs do not exceed the number of data [ECG leads]).

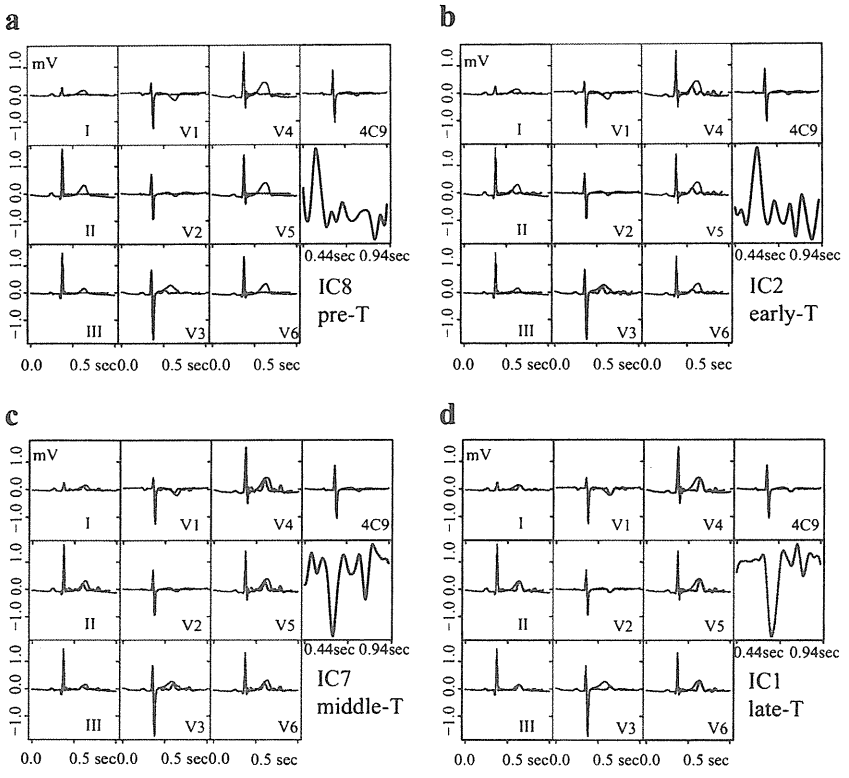

Figure 3. Results of independent component analysis (ICA) and inverse ICA in a normal subject. Four ICs constituting the normal T wave are represented in red waveforms in the second row of the fourth column of each part. Ten ICs were numbered in the order of appearance not on the T wave but in the results of the ICA. In all 30 normal subjects, the T wave included 4 ICs. Also shown are the results of inverse ICA. The blue waveforms represent the original ECG, and the red waveforms represent the distribution of each IC on the original leads, making it possible to recognize the origin of each IC on the original ECG. **a**, The waveform (red solid line) displays IC8. IC8 exists in the early phase of IC2 (early-T) in V3 and V4 (named *pre-T*). This IC was not always observed in the normal ECG. When absent, a small positive wave (last-T) appeared instead of pre-T. **b**, IC2 became the maximum in the vicinity of V3 and V4 and formed the early phase of the T wave (named *early-T*). **c**, IC7 occupied the area between IC2 (early-T) and the IC1 (late-T) (named *middle-T*). **d**, The second half of the T wave comprised IC1 (named *late-T*). IC1 is the major component of the V4 to V6 waveforms. IC indicates independent component.

in Figures 4 and 5 and online-only Data Supplement Figures 4 and 5.

The origins of the extra ICs determined by i-ICA in each patient with LQTS are listed in the Table. In most cases, the origin of ExT1 was the middle part of the T wave in V1 to V6, with the maximum origin in V2 to V5, and that of ExT2 was the late phase of the T wave mainly in V3 to V6. In cases with 3 extra ICs, the origin of ExT3 was exclusively the last part of the T wave mainly in V1 and sometimes in the left precordial leads. Among patients with the same gene mutation type (mainly family members), the constitution of the T wave was similar to one another; for example, the 3 subjects with the mutation V254M and the 2 with R518G showed similar ICs and their origins as well as the same type of T wave described by Zhang et al[2] (Table).

Even among 13 patients with LQT1 who were being treated with a β-blocker, 4 of whom also were being treated with verapamil or mexiletine, ≥5 ICs were extracted. In those with apparently normal QT intervals (patients 16, 19, and 20), extra ICs also were extracted. Patient 20 (Table) with normal QTc values under treatment with a β-blocker is presented in Figure 4 (see also online-only Data Supplement Figure 4). On the other hand, among 13 symptomatic patients, 5 ICs, 6 ICs, and 8 ICs were extracted from 9, 3, and 1, respectively, indicating that the number of extra ICs was not related to susceptibility to arrhythmias.

The classification of the types of T-wave morphology according to Zhang et al[2] are presented in the Table. Patients with the broad-based or normal-appearing T-wave morphologies tended to have 5 ICs, and those with the infantile or bifid ones tended to have 6 ICs (Table).

Discussion

The present study demonstrated for the first time, to our knowledge, that the T wave in normal subjects consists of 4 ICs, whereas those in LQTS comprised ≥5 (mostly 6) ICs, when ICA is applied to the T-wave area (ie, from the J point to the onset of the next P wave). In other words, ≥2 extra components were detected in LQTS in addition to the normal ICs present in LQTS (early-T, middle-T, and late-T). In LQTS with 5 ICs, summation of early-T, middle-T, and late-T made a distinct wave, and that of the other 2 waves (ExT1 and ExT2) provided another distinct wave. These 2 summated waves clearly divided each other. Therefore, the number of ICs of normal T waves was considered 3 instead of 4, and the other 2 waves were considered extra. Similarly, the T wave comprised 3 normal ICs and 3 extra ICs in LQTS with 6 ICs. It is noteworthy that patients with LQTS were clearly differentiated from normal subjects by the number of ICs. Furthermore, patients with LQT1 who showed normal QT intervals on the surface ECG (patients 16, 19, and 20) (Figure 4, Table) or those who were taking β-blockers also had additional ICs of the T wave (Table). However, unbiased estimates of the sensitivity and specificity of the method for the differentiation between patients with LQT1 and normal subjects should be obtained in an independent validation group with a large number of subjects.

We arbitrarily termed each T-wave component detected in the normal subjects as *pre-T*, *early-T*, *middle-T*, and *late-T*, and those observed only in patients with LQT1 as *ExT1*, *ExT2*, and *ExT3*...*ExTn*. The additional ICs were demonstrated by i-ICA to be located largely in the middle (ExT1) and late phase (ExT2 and ExT3) of repolarization, forming the second half or the last part of the T wave. The origin of ExT1

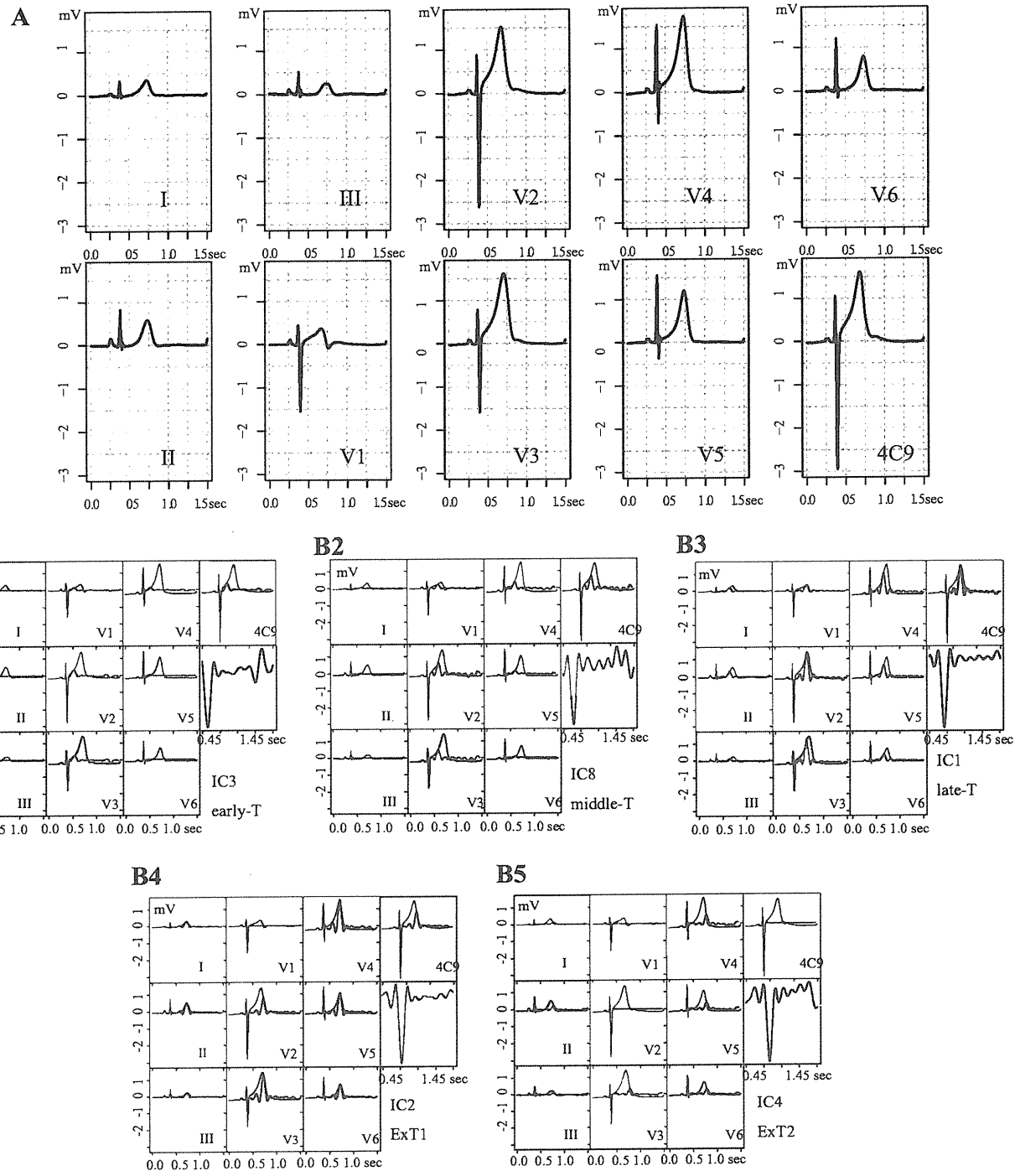

Figure 4. A typical case of LQT1 with 5 ICs (patient 20) (see Table). **A**, The 12-lead standard ECG, showing normal QTc (426 ms) and normal T-wave morphology. **B**, Results of independent component analysis (ICA) and inverse ICA. Although a β-blocker was being administered and the QT interval was normal, 5 ICs were extracted. The seventh-time ICA of the SD 0.7 group of fk22d6 was assumed to be the best model according to the rule described in the Methods section. The waveforms here are presented in the same way as in Figure 3. **B1**, IC3 was early-T, similar to that observed in normal T. **B2**, IC8 existed between IC3 (early-T) and IC1(late-T), and was named *middle-T* as in normal T. **B3**, IC1 formed the second half of the T wave in V1 to V2 and the middle part or the first half of the T wave in V3 to V6 (named *late-T*). **B4**, IC2 appeared later than IC1 (late-T) as the fourth wave in the time series, showing the maximum value at V4, and formed the latter half of left precordial leads (named *ExT1*). **B5**, IC4 appeared later than IC2 (ExT1) (named *ExT2*) as an inverted T wave with a small amplitude in V1. The maximum amplitude was observed in V4. It was confirmed to be located over V3 to V6 on the original ECG. IC indicates independent component.

was estimated to be widely distributed to V1 to V6 and those of ExT2 and ExT3 were mainly to V3 to V6, suggesting the presence of many myocardial cells that express malfunctional potassium channels due to *KCNQ1* mutation in the left ventricle.

Although the origins of extra ICs could not be clearly confined to a specific area, this distribution tendency is consistent with the results of a canine model study in which after-contraction that precedes torsade de pointes arises in the left ventricle.[16]

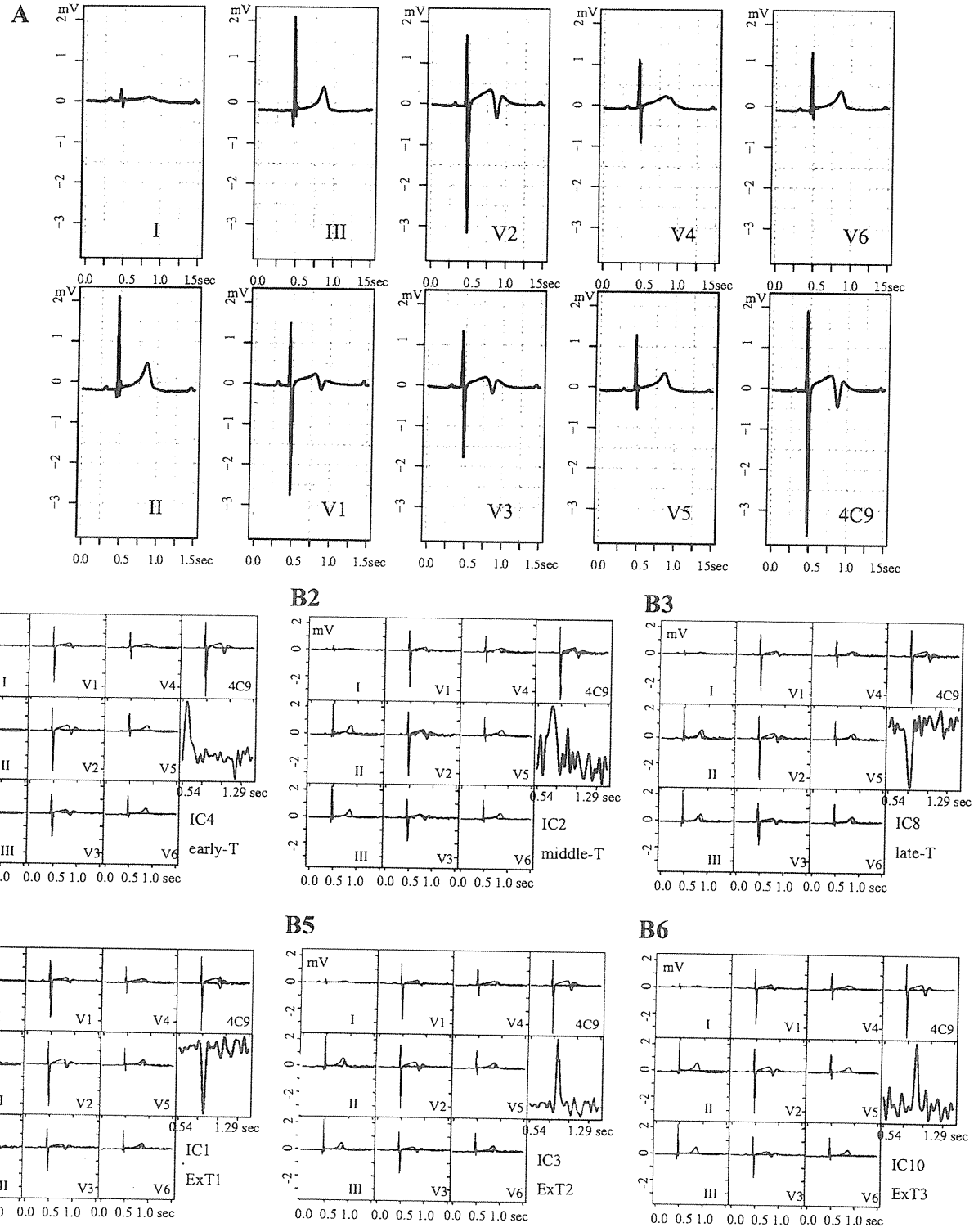

Figure 5. A typical case of LQT1 with 6 ICs (patient 13) (see Table). **A**, The 12-lead standard ECG showing prolonged QTc (488 ms). **B**, Results of independent component analysis (ICA) and inverse ICA. The seventh-time ICA of the SD 0.7 group of la20d5 by the mclust method was selected for the best model of this LQTS according to the rule described in the Methods section. The waveforms in each part are presented in the same way as in Figure 3. **B1**, IC4 was early-T, appearing as the first small wave in the right precordial leads similar to that observed in normal T. **B2**, IC2 was middle-T, being located at the position from the early to middle period in the right precordial leads. **B3**, IC8 appeared as the third wave, forming the latter half of the T wave in the right precordial leads (late-T). **B4**, IC1 appeared as the fourth wave and formed the inverted T wave in the right precordial leads as well as in the latter half of the T wave in the left precordial leads. This IC was ExT1 not observed in normal T waves. **B5**, IC3 appeared sequentially as the fifth wave, forming the latter half of the inverted T wave in the right precordial leads V1 to V2 as well as in the last part of T wave in the left precordial leads. This IC was ExT2 and not observed in normal T waves. **B6**, IC10 appeared as the sixth single wave, comprising the last triangle portion of the T wave in the right precordial leads. This IC was ExT3 and not observed in the normal T waves. Although the normal T wave in some healthy control subjects resembled the Aries symbol in lead V2, the last triangle existed not in normal subjects but in patients with LQTS as a single IC. IC indicate independent component.

Recent discovery of many types of mutations of genes encoding myocardial ion channels has encouraged channel-based discussion about T-wave morphology.[4] Nevertheless, the clinical usefulness of the T-wave morphology in the diagnosis of LQTS has been limited because quantitative analysis cannot be easily applied. In 1995, Moss at al[3] demonstrated for the first time the genotype-specific morphology of the T wave. In 2000, Zhang et al[2] reported more complex diversity in T-wave morphology in each type of LQTS as described earlier. Accordingly, we tried to classify the present study patients into the template. The infantile-type T wave could only be detected in 1 patient in our study who was aged <5 years. Although the other 3 types of T wave were identified, the wave morphology was rather similar to that of LQTS type 2 (hERG mutation), with a bifid T wave in 3 patients.[17] This classification was mostly qualitative and depended on the skill and experience of the investigator, and it was not necessarily easy to classify the patients convincingly. However, it is intriguing that the types of T-wave morphology described by Zhang et al[2] were associated considerably with the number of ICs in the present study. Furthermore, it is noteworthy that even in the "normal" T-wave types with normal QTc values, extra ICs were extracted (Figure 4, online-only Data Supplement Figure 4).

Among the quantitative methods of analysis, QT dispersion on the 12-lead ECG is one of the most common parameters applied to LQTS.[18] However, the value of QT dispersion remains clouded because determination of the T-wave offset is not always possible, and it is possible that some of the QT intervals measured on the different ECG leads are just different projections of a common current dipole. Assessment of monophasic action potentials at various ventricular sites is a more definitive way to evaluate the heterogeneity of ventricular repolarization,[16] but it is an invasive method using an electrode during catheterization. Recently, Kanters et al[16] applied the Hill equation to T-wave morphology analysis. Furthermore, Vaglio et al[19] reported an automatic algorithm for the quantification of T-wave morphology. Both methods could discriminate LQT1 from LQT2 and, interestingly, revealed that the repolarization process shifted to the later phase in LQT1 than LQT2. This tendency is consistent with the present results that extra ICs mainly constitute the second part of the T wave.

As a multivariate analysis of inhomogeneity of ventricular repolarization, the principal component analysis has been applied for the assessment of T-wave morphology in LQTS by some investigators,[20,21] the results of which demonstrated its usefulness in distinguishing abnormal from normal repolarization processes such that a high second/first eigenvector ratio predicts increased inhomogeneous repolarization.[20,21] Principal component analysis also was reported to be useful in prediction of cardiovascular mortality.[22] So far, ICA has not been applied for analysis of the repolarization process in LQTS. It is noteworthy that ≥2 extra ICs, which were not extracted from T waves of normal subjects, were demonstrated in all patients with LQT1, including those with normal QTc values or those taking β-blockers. Compared with the earlier methods discussed previously, ICA tends to be influenced more by the presence of noise, making it difficult to exclusively extract significant ICs. However, the wavelet thresholding technique for noise reduction combined with the sophisticated mathematical techniques for the best model selection in ICA proved to be useful for the diagnosis of LQTS. Although the complicated data analysis procedure (including waveform approximation and the best model selection in ICA) can be performed almost automatically (in the order of the flow chart presented in online-only Data Supplement Figure 1), it would be preferable in future studies to see results from an analyst who is blinded with regard to the LQTS or normal status of the study subjects and would help to further validate the usefulness of the method.

It would be intriguing to see whether the number of ICs reflects the severity of the disease; that is, those patients who experience syncope or ventricular arrhythmias tend to have ≥3 extra ICs. Although we examined only patients with LQT1 in this study to simplify interpretation of the results of the newly applied methods, further studies are needed to explore this hypothesis in a large number of subjects, including patients with other mutations of LQTS, especially LQT2 or LQT3.

Disclosures

None.

References

1. Vincent GM, Timothy KW, Leppert M, Keating M. The spectrum of symptoms and QT intervals in carriers of the gene for the long QT syndrome. *N Engl J Med.* 1992;327:846–852.
2. Zhang L, Timothy KW, Vincent GM, Lehmann MH, Fox JLC, Giuli LC, Shen J, Splawski I, Priori SG, Compton SJ, Yanowitz F, Benhorin J, Moss AJ, Schwartz PJ, Robinson JL, Wang Q, Zarebra W, Keating MT, Towbin JA, Napolitano C, Medina A. Spectrum of ST-T wave patterns and repolarization parameters in congenital long-QT syndrome: ECG findings identify genotypes. *Circulation.* 2000;102:2849–2855.
3. Moss AJ, Zareba W, Benhorin J, Locati EH, Hall WJ, Robinson JL, Schwartz PJ, Towbin JA, Vincent GM, Lehmann MH. ECG T-wave patterns in genetically distinct forms of the hereditary long QT syndrome. *Circulation.* 1995;92:2929–2934.
4. Antzelevitch C. Molecular genetics of arrhythmias and cardiovascular conditions associated with arrhythmias. *J Cardiovasc Electrophysiol.* 2003;14:1259–1272.
5. Cichocki A, Amari S. *Adaptive Blind Signal and Image Processing.* New York, NY: John Wiley & Sons; 2002.
6. Hyvärinen A, Karhunen J, Oja E. *Independent Component Analysis.* New York, NY: John Wiley & Sons; 2001.
7. Comon P, Jutten C. *Handbook of Blind Source Separation.* Burlington, MA: Academic Press; 2010.
8. Learned-Miller EG, Fisher JW III. ICA using spacings estimates of entropy. *J Mach Learn Res.* 2003;4:1271–1295.
9. Whitcher B. waveslim: Basic wavelet routines for one-, two- and three-dimensional signal processing. 2010; R package version 1.6.4. http://cran.r-project.org/web/packages/waveslim/index.html. Accessed April 15, 2011.
10. Gençay R, Schçuk F, Whicher B. An *Introduction to Wavelets and Other Filtering Methods in Finance and Economics.* San Diego, CA: Academic Press; 2002:112–116.
11. Yanai S, Ishikawa Y, Fuse S, Tsutsumi H. Inverse independent component analysis facilitates clarification of the accessory conductive pathway of Wolf-Parkinson-White syndrome electrocardiogram. *Pediatr Cardiol.* 2008;30:59–69.
12. Amari S, Cichocki A, Yang HH. A new learning algorithm for blind signal separation. In: Touretzky D, Mozer M, Hasselmo M. eds. *Advances in Neural Information Processing Systems 8.* Cambridge, MA: MIT Press; 1996:757–763.
13. Cardoso JF. High-order contrasts for independent component analysis. *Neural Comput.* 1999;11:157–192.

14. Fraley C, Raftery A. mclust: Model-based clustering/normal mixture modeling. 2010; R package version 3.4.8. http://cran.r-project.org/web/packages/mclust/index.html. Accessed April 15, 2011.
15. Everitt B. *An R and S-PLUS Companion to Multivariate Analysis*. London, UK: Springer-Verlag; 2007:128–134.
16. Gallacher DJ, Van de Water A, van der Linde H, Hermans AN, Lu HR, Towart R, Volders PG. In vivo mechanisms precipitating torsades de pointes in a canine model of drug-induced long-QT1 syndrome. *Cardiovasc Res*. 2007;76:247–256.
17. Kanters JK, Fanoe S, Larsen LA, Thomsen PEB, Toft E, Christiansen M. T wave morphology analysis distinguishes between KvLQT1 and HERG mutations in long QT syndrome. *Heart Rhythm*. 2004;3:285–292.
18. Surawicz B. Will QT dispersion play a role in clinical decision-making? *J Cardiovasc Electrophysiol*. 1996;7:777–784.
19. Vaglio M, Couderc JP, McNitt S, Xia X, Moss AJ, Zareba W. A quantitative assessment of T-wave morphology in LQT1, LQT2, and healthy individuals based on Holter recording technology. *Heart Rhythm*. 2008; 5:11–18.
20. Priori SG, Mortara DW, Napolitano C, Diehl L, Paganini V, Cantù F, Cantù G, Schwartz PJ. Evaluation of the spatial aspects of T-wave complexity in the long-QT syndrome. *Circulation*. 1997;96:3006–3012.
21. Extramiana F, Haggui A, Maison-Blanche P, Dubois R, Takatsuki S, Beaufils P, Leenhardt A. T-wave morphology parameters based on principal component analysis reproducibility and dependence on T-offset position. *Ann Noninvasive Electrocardiol*. 2007;12:354–363.
22. Okin PM, Devereux RB, Fabsitz RR, Lee ET, Galloway JM, Howard BV. Principal component analysis of the T wave and prediction of cardiovascular mortality in American Indians. The Strong Heart Study. *Circulation*. 2002;105:714–719.

Pediatr Cardiol (2011) 32:846–848
DOI 10.1007/s00246-011-9978-8

CASE REPORT

Focal Atrial Tachycardia Originating From Inside the Inferior Vena Cava Late After Surgical Repair of Congenital Heart Defects

Yoshiaki Kato · Hitoshi Horigome · Miho Takahashi-Igari · Kazutaka Aonuma

Received: 25 October 2010 / Accepted: 22 March 2011 / Published online: 10 April 2011

Abstract An 11-year-old girl presented with focal atrial tachycardia (AT) originating from inside the inferior vena cava (IVC). Sustained AT appeared 10 years after surgical repair of the congenital heart defects. Focal AT was successfully eliminated with radiofrequency application at the earliest activation site, about 8 mm below the IVC right atrium junction. These findings suggested the existence of an electrically continuous myocardial extension in the IVC and a real risk of AT originating from IVC late after cardiopulmonary bypass with IVC cannulation.

Keywords Atrial tachycardia · Congenital heart defect · Inferior vena cava · Myocardial extension

The foci of right focal atrial tachycardia (AT) are commonly distributed around the crista terminalis, coronary sinus ostium, parahisian region, tricuspid annulus, superior vena cava, and right atrial appendage [4, 8, 9]. However, the inferior vena cava (IVC) is considered a rare source of atrial arrhythmia. We report the case of an 11-year-old girl with focal AT originating from inside the IVC, which emerged 10 years after surgery for a congenital heart defect.

Y. Kato (✉) · H. Horigome · M. Takahashi-Igari
Department of Child Health, Graduate School of Comprehensive Human Sciences, University of Tsukuba, 1-1-1, Tennnodai, 305-8575 Tsukuba, Ibaraki, Japan
e-mail: yoshiakiaisho@hotmail.com

K. Aonuma
Division of Cardiology, Department of Internal Medicine, Graduate School of Comprehensive Human Sciences, University of Tsukuba, 1-1-1, Tennnodai, 305-8575 Tsukuba, Ibaraki, Japan

Case Report

An 11-year-old girl was admitted to our hospital for management of AT. She had undergone percutaneous balloon angioplasty for coarctation of the aorta at the age of three months and closure of a ventricular septal defect through the transpulmonary approach without right atriotomy at the age of 14 months. A cannula (16 Fr) for cardiopulmonary bypass was inserted into the IVC at the level of the IVC right atrium (RA) junction.

The girl's clinical course after surgery was uneventful until the age of 11, when tachycardia occurred. A surface electrocardiogram (ECG) showed AT with deep negative P-waves in the inferior leads (Fig. 1). An intravenous infusion of adenosine triphosphate induced transient atrioventricular block but was ineffective in terminating the AT. The atrial rate gradually slowed to approximately 100 bpm after an intravenous infusion of verapamil. Finally, AT converted to sinus rhythm 2 days after the start of oral propranolol.

An electrophysiologic study showed no evidence of a dual atrioventricular nodal pathway or atrioventricular accessory pathway. No arrhythmia was induced by pacing protocols in the baseline state. However, during intravenous infusion of isoproterenol (2 μg/min), AT was induced, with atrial burst pacing at a cycle length of 400 ms. A bolus infusion of adenosine triphosphate 20 mg (0.5 mg/kg) induced transient two-to-one atrioventricular block.

An electroanatomical mapping system (CARTO XP; Biosense Webster Inc., Diamond Bar, CA, USA) was used to determine the origin of AT. The activation map showed that the earliest activated site was the inside the IVC, about 8 mm below the IVC-RA junction (Fig. 2), and that the activation wave front spread centrifugally. Neither a

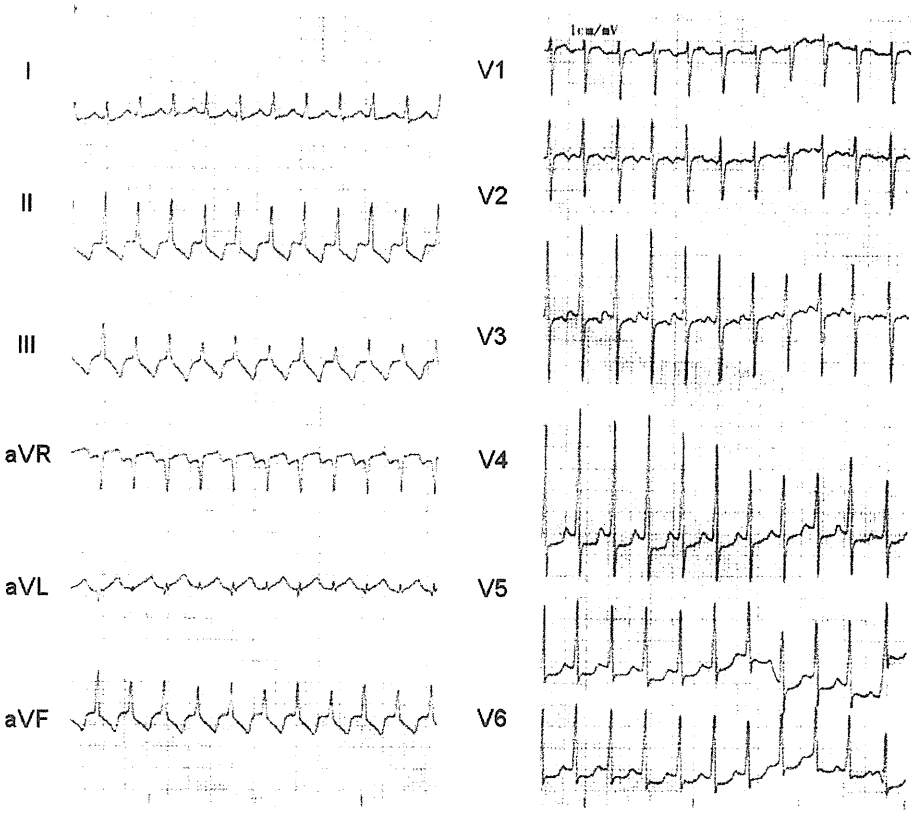

Fig. 1 Surface electrocardiography (ECG) showed atrial tachycardia (heart rate, 193 bpm) with deep negative P-waves and inverted T-waves in leads II, III, and aVF. Slight ST segment depression was recorded in the left precordial leads

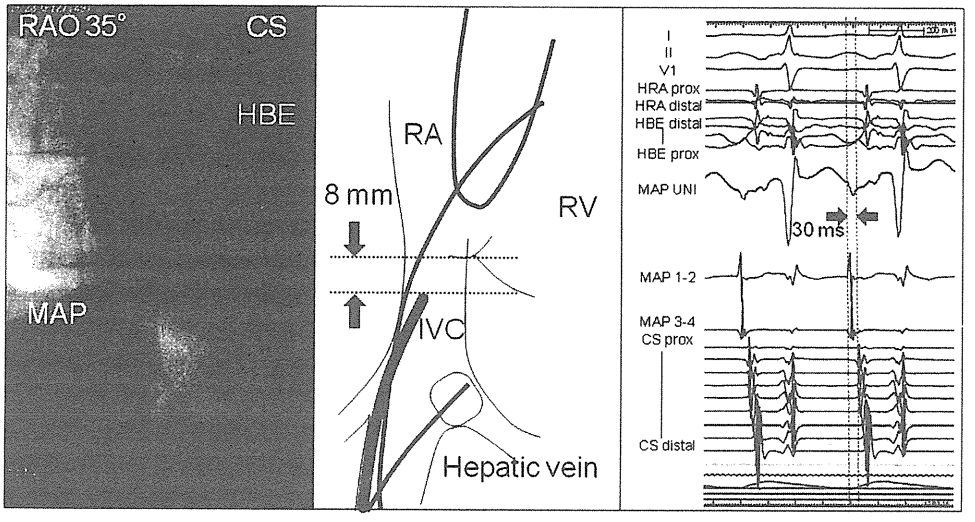

Fig. 2 *Left panel* Angiogram of the IVC (right anterior oblique view 35°) showing positions of catheters at the site of successful ablation. *Middle panel* Schema of angiogram showing the positioning of the ablation catheter 8 mm below the IVC-RA junction. *Right panel* Surface electrocardiography (ECG) and intracardiac recordings of the electrograms from the ablation catheter (MAP) located at the site of successful ablation. Bipolar activation (MAP 1-2) preceded P-wave onset by 30 ms, and the unipolar signal (MAP UNI) was entirely negative. *CS* coronary sinus, *HBE* His bundle electrogram, *HRA* high right atrium, *IVC* inferior vena cava, *MAP* mapping catheter, *RA* right atrium, *RV* right ventricle, *UNI* unipolar

double-potential nor an obvious low-voltage area was observed around the IVC-RA junction.

Radiofrequency application via a 3.5-mm-tip, open-irrigated catheter (THERMOCOOL; Biosense Webster) was delivered (power, 20 W; target temperature, 35°C) at the site of earliest activation (Fig. 2). After the radiofrequency application, AT could no longer be induced by the maximal stimulation program under isoproterenol. The patient was free of tachycardia during the next 12 months of follow-up evaluation without any medication.

Discussion

Knowledge gained from increasing experience with catheter ablation of atrial fibrillation shows myocardial extension into thoracic veins (pulmonary veins, superior vena cava, and coronary sinus) to be the major source of ectopic beats. However, the IVC is considered a rare source of atrial arrhythmia. Only five cases of atrial arrhythmia originating from the IVC have been reported [5–7, 10]. These reports suggest the presence of myocardial extension into the IVC.

Studies investigating the IVC indicate that the morphologic characteristics of myocardial extension in the IVC are similar to those involving the SVC [2, 3]. Although the frequency of myocardial extension in the IVC is similar to that in the SVC [3], arrhythmia originating from the IVC is clinically very rare compared with that originating from the SVC. Kholova and Kautzner [3] speculated that the frequent absence of an electrical connection between myocardial extension and RA due to discontinuity of myocardial fibers may explain the discordance between the morphologic and electrophysiologic characteristics of the IVC.

In the reported case, the electrophysiologic findings suggested the presence of an electrically connected continuous myocardial extension from RA to the focus of AT, which was located relatively deep inside the IVC. In contrast to the non-postsurgical focal AT, foci of postsurgical focal AT are distributed mainly near surgically created arrhythmogenic substrates such as the IVC cannulation site. However, the positional relation between the focus of AT and the cannulation site was ambiguous from the information on the bipolar voltage map of the IVC-RA junction. Chen et al. [1] reported that cardiomyocytes of SVC showed pacemaker activity and delayed after depolarization, suggesting implication of automaticity, triggered activity, or both in the arrhythmogenic activity in SVC.

In the reported case, myocardial extension in the IVC itself might have arrhythmogenicity by the same mechanism as that of atrial arrhythmia originating from SVC. It is possible that an arrhythmogenic substrate produced by cannulation provoked focal activation and that cannulation also altered the electrical connection of myocardial extension, enabling the electrical activation to propagate to RA. Although the real impact of cannulation on the emergence of AT needs to be analyzed further, these findings suggest that patients who undergo cardiopulmonary bypass using IVC cannulation could present in the future with AT originating from the IVC.

References

1. Chen YJ, Chen YC, Yeh HI, Lin CI, Chen SA (2002) Electrophysiology and arrhythmogenic activity of single cardiomyocytes from canine superior vena cava. Circulation 105:2679–2685
2. Hashizume H, Ushiki T, Abe K (1995) A histological study of the cardiac muscle of the human superior and inferior venae cavae. Arch Histol Cytol 58:457–464
3. Kholova I, Kautzner J (2004) Morphology of atrial myocardial extensions into human caval veins: a postmortem study in patients with and without atrial fibrillation. Circulation 110: 483–488
4. Kistler PM, Roberts-Thomson KC, Haqqani HM, Fynn SP, Singarayar S, Vohra JK, Morton JB, Sparks PB, Kalman JM (2006) P-wave morphology in focal atrial tachycardia: development of an algorithm to predict the anatomic site of origin. J Am Coll Cardiol 48:1010–1017
5. Mansour M, Ruskin J, Keane D (2002) Initiation of atrial fibrillation by ectopic beats originating from the ostium of the inferior vena cava. J Cardiovasc Electrophysiol 13:1292–1295
6. Mizobuchi M, Enjoji Y, Shibata K, Funatsu A, Yokouchi I, Kambayashi D, Kobayashi T, Nakamura S (2006) Case report: focal ablation for atrial fibrillation originating from the inferior vena cava and the posterior left atrium. J Interv Card Electrophysiol 16:131–134
7. Scavee C, Jais P, Weerasooriya R, Haissaguerre M (2003) The inferior vena cava: an exceptional source of atrial fibrillation. J Cardiovasc Electrophysiol 14:659–662
8. Tada H, Nogami A, Naito S, Suguta M, Nakatsugawa M, Horie Y, Tomita T, Hoshizaki H, Oshima S, Taniguchi K (1998) Simple electrocardiographic criteria for identifying the site of origin of focal right atrial tachycardia. Pacing Clin Electrophysiol 21:2431–2439
9. Toyohara K, Fukuhara H, Yoshimoto J, Ozaki N, Nakamura Y (2011) Electrophysiologic studies and radiofrequency catheter ablation of ectopic atrial tachycardia in children. Pediatr Cardiol 32:40–46
10. Yamane T, Miyazaki H, Inada K, Matsuo S, Miyanaga S, Date T, Abe K, Sugimoto K, Mochizuki S (2005) Focal source of atrial fibrillation arising from the ostium of the inferior vena cava. Circ J 69:756–759

10.5005/jp-journals-10009-1174

REVIEW ARTICLE

Screening of Fetal Heart for the Congenital Heart Diseases

[1]Yasuki Maeno, [2]Akiko Hirose

Division of Maternal and Perinatal Medical Center, Department of Pediatrics and Child Health
Kurume University, School of Medicine, Kurume, Japan

Correspondence: Yasuki Maeno, Division of Maternal and Perinatal Medical Center, Department of Pediatrics and Child Health Kurume University, School of Medicine, 67 Asahi-mach, Kurume-830-0011, Japan, e-mail: yasukim@med.kurume-u.ac.jp

ABSTRACT

Screening of the congenital heart disease (CHD) is one of the most important techniques in prenatal ultrasonographic examination. Step by step screening methods for taking account for the level of screener, especially in the area with poor detection rate, is needed for starting effective fetal CHD screening. In this review, the fetal cardiac screening is divided into two methods accounting for steps for learning screening technique; the basic screening and the advanced screening. Basic screening is a simple method even for the one who is not familiar to the cardiac anatomy. The goal of this basic screening is to detect most of the ductal dependent lesions including transposition of the great arteries. For the basic screening, 'location' and 'size' of the heart and vessels are checked in standard four-chamber view and three-vessel view. Advanced screening is a screening for detecting all fetal CHDs, including total anomalous pulmonary venous return. For the advanced screening, the side of the heart is defined, and then the 'detail anatomy' and the 'function and blood flow' are assessed in all standard screening views, including one fetal abdominal transverse view and three fetal chest transverse views, such as four-chamber, three-vessel and three-vessel and trachea view.

Keywords: Fetal echocardiography, Fetal screening, Congenital heart disease.

INTRODUCTION

Screening of the congenital heart disease (CHD) is one of the most important techniques in prenatal ultrasonographic examination. Recent conventional ultrasound equipment can visualize cardiac anatomy *in utero* from 16 weeks of gestation even by the transabdominal approach.[1-3] Referral to the tertiary care center after effective screening of fetal CHD can make it possible to diagnose detail anatomical abnormality and to plan appropriate perinatal management. Prenatal diagnosis of CHD can improve the outcome of the fetuses with CHD.[4]

For the screening, detail anatomical assessment of the CHD is not needed. The purpose of the screening is to detect the fetuses with possibility of having CHD, and to refer to the fetal cardiac center. Several methods with simple technique have been proposed for effective screening. However, learning the technique for obtaining the images in sufficient quality still requires certain training, hence, the detection rate of fetal CHD is varied between the areas.[5] Different condition of the region and country, such as medical system and political environment, may be one of the causes of difficulty for establishing effective fetal CHD screening program. An issue for poor detection rate in some regions seems to be caused by the feeling of difficulty for starting fetal cardiac screening for the screeners who are not familiar to the fetal echocardiography. Hence, step by step screening methods for taking account for the level of screener in certain area is needed for increasing the area for starting fetal CHD screening.

In this review, we present the fetal cardiac screening dividing into two methods account for step for learning screening technique; the basic screening and the advanced screening. The basic screening is a very simple method even for the screener who is not familiar to the somewhat complicated cardiac anatomy. The advanced screening is the method of goal for all fetal sonographic screener who is trying to detect all major CHD.

INDICATIONS OF THE SCREENING

Appropriate ultrasonographic screening of fetal CHD is indicated for all pregnant women.[1-3] Unlike in the newborn period, the presence of severe cardiac disease in the fetus, such as heart murmur and cyanosis, cannot be detected by physical examination. Therefore, fetal ultrasonographic screening of a completely healthy mother with an uneventful pregnancy is the only method of identifying the majority of cases of congenital heart disease *in utero*.

The first screening ultrasound should be performed at approximately 20 weeks of gestation, if termination of pregnancy is to be considered as an option in complex cardiac problems, and there is some restriction in gestational age by law for termination. Screening has to be performed sufficiently early to make it possible to refer the case to a fetal cardiac center and to allow the parents to make their decision. The second screening for fetal CHD should be performed at approximately 30 weeks of gestation because some cardiac abnormalities develop more obvious structural abnormality in later gestation.

CONCEPT OF BASIC AND ADVANCED SCREENING

Basic Screening

Basic screening is a simple method even for the one who is not familiar to the cardiac anatomy. This screening method can be

applied when the detection rate of fetal CHD is low in that region. The goal of this basic screening is to detect most of the ductal dependent lesions including transposition of the great arteries (TGA). Although, standard four-chamber view and three-vessel view are used in this basic screening, the check point is only limited to the location and size of the heart and vessels. Checking the detail anatomy of the heart is not required if the purpose of the screening is limited to detect major CHD, except total anomalous pulmonary venous drainage (TAPVR).

Advanced Screening

Advanced screening is a screening for detecting all fetal CHDs as much as possible, including TAPVR. First, the side of the heart is defined. Then, all standard screening views including one fetal abdominal transverse view and three fetal chest transverse views are checked. In all view, detail anatomy and function and blood flow of the heart and vessels, in addition to the location and size, are checked.

FETAL HEART SECTIONS FOR SCREENING CHD

For the fetal heart screening, defining the side of the heart is needed (advanced screening). The other views are four transverse images of the fetus. First one is an abdominal transverse image of the fetus, and remaining is three simple transverse images of the fetal chest, such as the four-chamber, the three-vessel, and the three-vessel and trachea view (Figs 1 and 2). In each view, checking points are divided into location, size, detail anatomy and function and blood flow.

Defining the Side of the Heart

Since conventional ultrasound image is two-dimensional in nature, the side of the image depends on the probe direction, and cannot be interpreted from the 2D image itself. Hence, the side of the fetal heart has to be defined at the beginning of the examination (Fig. 3).[6] A longitudinal section of the fetal chest or abdomen is imaged with the fetal head positioned at the right side of the screen. Then, a fetal transverse section is imaged by rotating the probe by 90° clockwise. Regardless of fetal position,

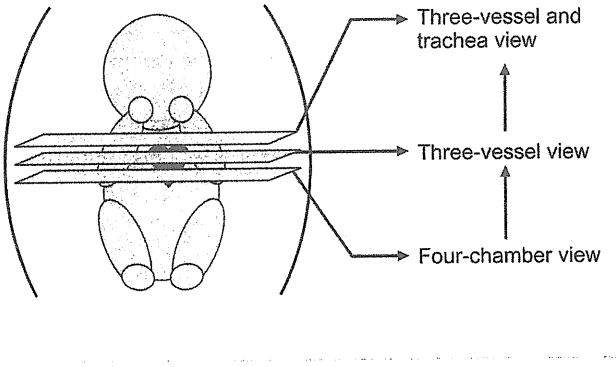

Fig. 1: Three transverse sections of the fetal chest, four-chamber, three-vessel, and three-vessel and trachea view

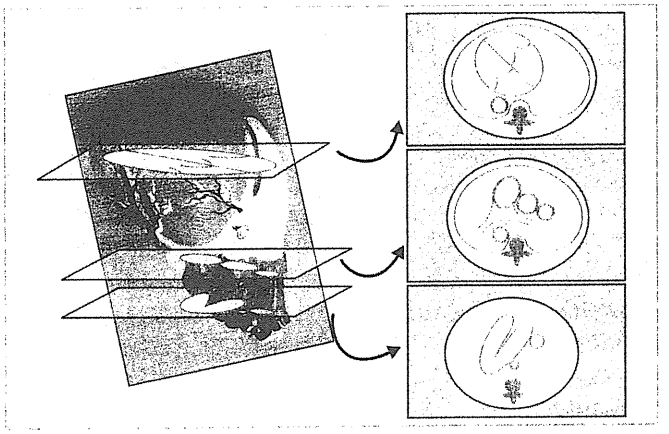

Fig. 2: Location of the each transverse section of the fetal heart

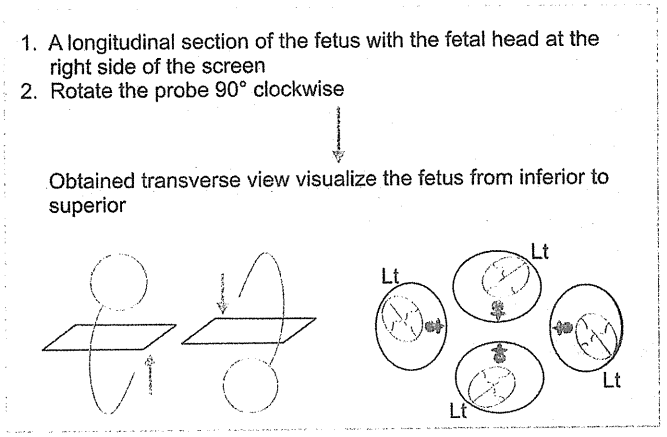

Fig. 3: Step for deciding the side of the fetal heart

the obtained image should be used to visualize the fetus from inferior to superior. In this view, the side of the heart and stomach should be defined whether it is left side (normal) or right side (abnormal). The easy way to interpret the side of the heart is that the heart is rotated clockwise after the probe is rotated clockwise.

Transverse Section of the Fetal Abdomen

Assessment of location is sufficient in this view. The stomach is left side, same as the fetal heart. In front of the fetal spine, the descending aorta (dAo) is positioned left side, and the superior vena cava (SVC) is positioned right and anterior to the dAo.

Four-Chamber View

A four-chamber view of the fetal heart is obtained by a transverse section of the lower part of the fetal chest (Figs 2, 4 and 5). This four-chamber view can detect more than 50% of CHDs, such as single ventricle, hypoplastic left ventricle (Fig. 6) and Ebstein's anomaly (Figs 7 and 8).

The location and size in this four-chamber view should be assessed for basic screening (Figs 4 and 5). There are three check points in each of location and size assessment in four-chamber view. For the location assessment, the fetal heart is positioned at left side of the chest, and the heart axis is about 45%. The dAo is positioned at the left anterior to the spine. For

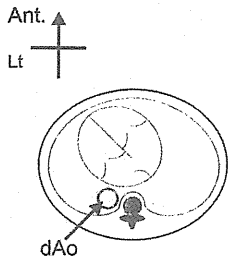

Location
1. The heart is located at the left side
2. The heart axis is about 45°
3. dAo is located at the left, anterior to the spine

Size
1. The heart occupies approximately one-third of the thorax
2. There are two atria of equal size
3. There are two ventricles of equal size

Anatomy
The ventricular septum, crux of the heart, the two atrioventricular valves, the foramen ovale, the pulmonary veins, papillary muscle

Function
ventricular contraction, valve regurgitation

Fig. 4: Check list of four-chamber view

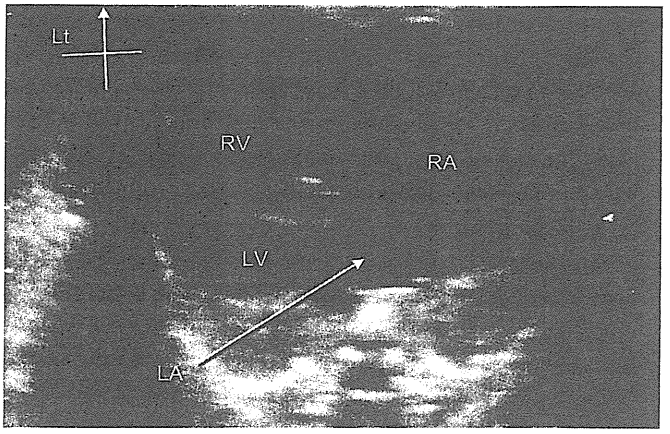

Fig. 7: A four-chamber view of a fetus with Ebstein's anomaly. The heart is quite enlarged and fills almost the entire chest. The right atrium (RA) is enlarged because of severe tricuspid valve regurgitation. LA, left atrium; LV, left ventricle; RA, right atrium; RV, right ventricle

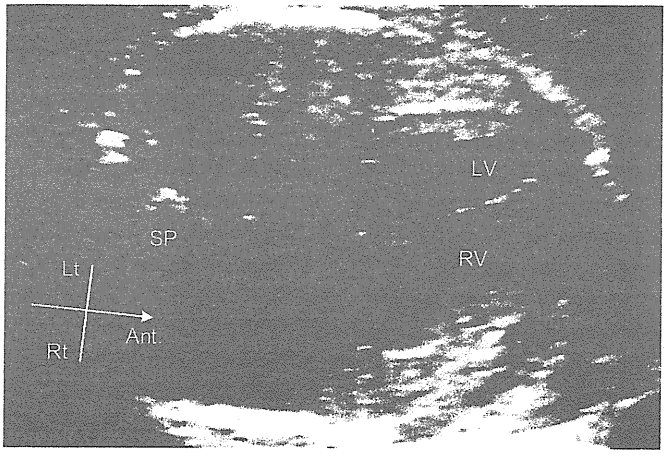

Fig. 5: Fetal echocardiographic image of four-chamber view

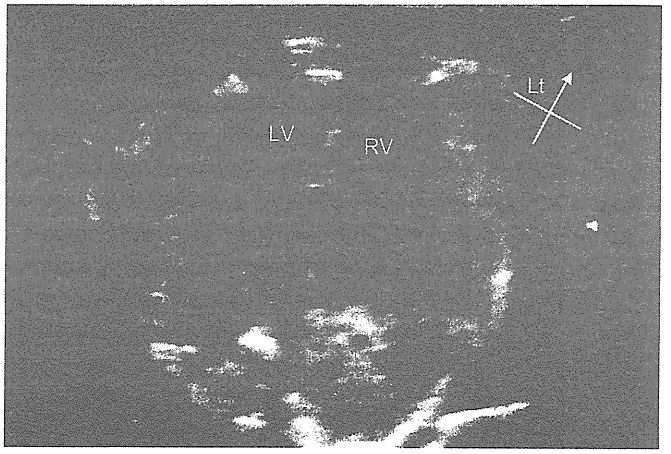

Fig. 8: A four-chamber view of a fetus with atrioventricular septal defect. A large one common atrioventricular valve is revealed, and the crux of the heart is not formed. LV, left ventricle; RV, right ventricle

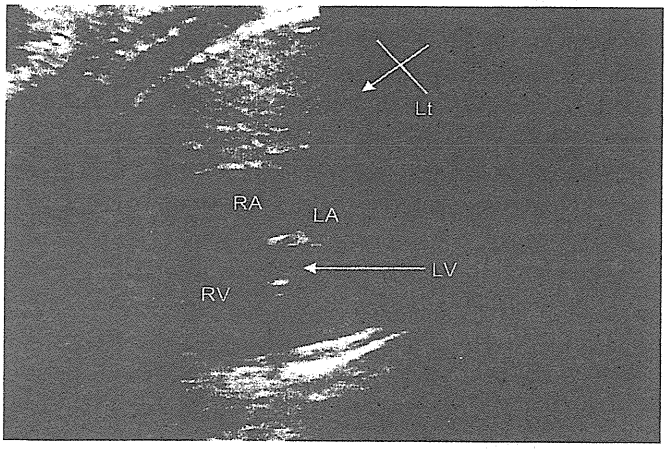

Fig. 6: A four-chamber view of a fetus with hypoplastic left heart syndrome. The left ventricle (LV) is small and endocardium of LV is high echogenic due to endocardial fibroelastosis. LA, left atrium; LV, left ventricle; RA, right atrium; RV, right ventricle

the size assessment, the fetal heart occupied approximately 1/3rd of the fetal chest. There are two atria of equal size, and two ventricles of equal size.

The assessment of the detail anatomy and the function and blood flow is included for advanced screening. Sufficient knowledge of cardiac anatomical feature and usage of color Doppler are required for these assessments. For the assessment of the detail anatomy, the crux of the heart, the ventricular septum, flap of the foramen ovale, the atrioventricular valves, the pulmonary veins and the papillary muscles should be checked. Next, function and blood flow should be assessed. Good contraction of each ventricle is carefully checked. By the color Doppler flow, location of the pulmonary venous return can be confirmed. In addition, regurgitant jet at the mitral valve and tricuspid valve can also be detected.

Three-Vessel View

The three-vessel view can be obtained by sweeping superior from the four-chamber view (Figs 2, 9 and 10).[7] This view can detect abnormal connections between the ventricles and the great arteries, such as TGA (Fig. 11) and tetralogy of Fallot.

The location and the size in this three-vessel view should be assessed for basic screening (Fig. 9). There is a just one check point in each of location and size assessment in three-vessel view. For the location assessment, three vessels are straightly aligned from left anterior to the right posterior. In another ward, the most anterior vessel is located at the most

left side. For the size assessment, the vessel size is aligned from the largest to the smallest when the straightly aligned vessels are followed from left anterior to right posterior. The most left anterior side vessel, the main pulmonary artery, is of the largest size. The central vessel, the ascending aorta (aAo), is medium in size. The most right posterior side vessel, the superior vena cava, is the smallest.

In order to assess the location of the three vessels with confidence, sweeping movement of images from the four-chamber view to the three-vessel view is useful. Using this moving image with sweeping, connection from both the ventricle to the vessels is visualized, so that the location of the vessel is clearly assessed. The ascending aorta and the main pulmonary arteries have cross relationship in normal heart (Fig. 12). By this sweeping movement, the connection from the left ventricle to the ascending aorta is first visualized. The ascending aorta is located posteriorly to the right ventricle and running from left to the right side according to the sweeping movement of the images. After this, the connection from the right ventricle to the main pulmonary artery is visualized. The main pulmonary artery is located anteriorly to the aorta just posterior to the chest-wall, and running from right to left side according to the sweeping movement of the images. The most obvious abnormality of this cross relationship of the two vessels is TGA. For the fetus with TGA, two vessels are aligned to parallel and straight rather than cross (Fig. 13), making the most left-side vessel, the main pulmonary artery, located posteriorly to the right sided ascending aorta (Fig. 11).

The assessment of the detail anatomy and the function and blood flow are required for advanced screening. For the detail anatomy assessment, the most left side vessel, the main pulmonary artery, is branching pulmonary arteries. It also connected to descending aorta via the ductus arteriosus at a slightly superior slice of three-vessel view. For the blood flow assessment, color Doppler flow reveals laminar flow in both the main pulmonary artery and the ascending aorta, directed from anterior to the posterior.

Three-Vessel and Trachea View

The last screening view, three-vessel and trachea view (Figs 14 and 15), can be obtained by farther superior sweep from three-vessel view.[8] This view may be included to the advanced

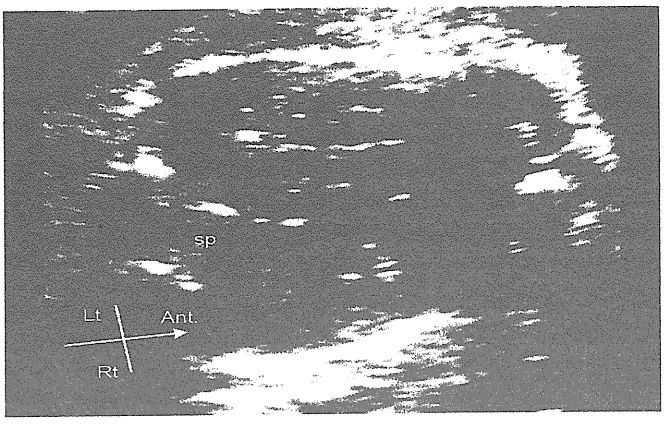

Fig. 10: A fetal echocardiographic image of three-vessel view

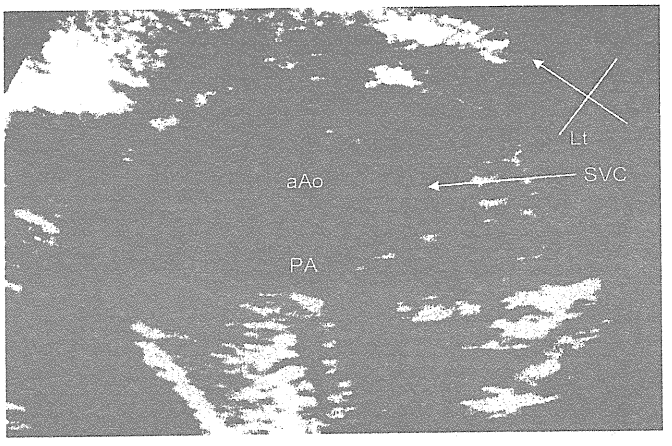

Fig. 11: A three-vessel view reveals a right anterior ascending aorta (aAo) and left posterior main pulmonary artery (PA). ant, anterior; SVC, superior vena cava

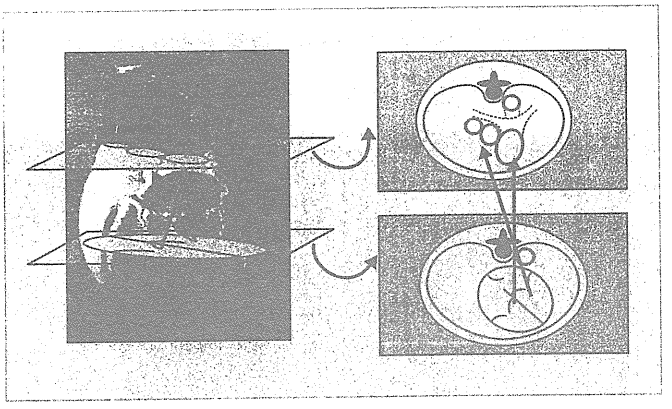

Fig. 12: Normal cross connection of the ventricles and the great vessels

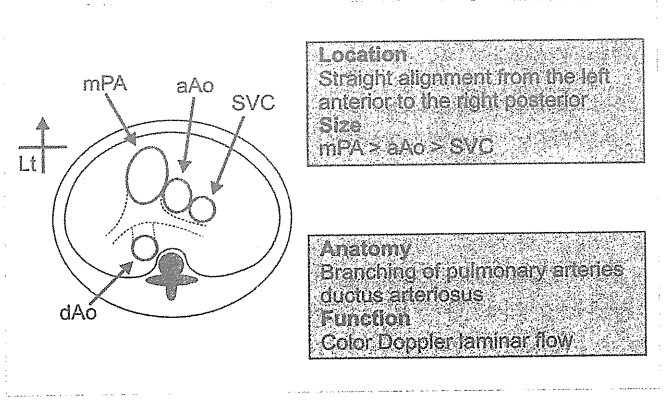

Fig. 9: Check list of three-vessel view

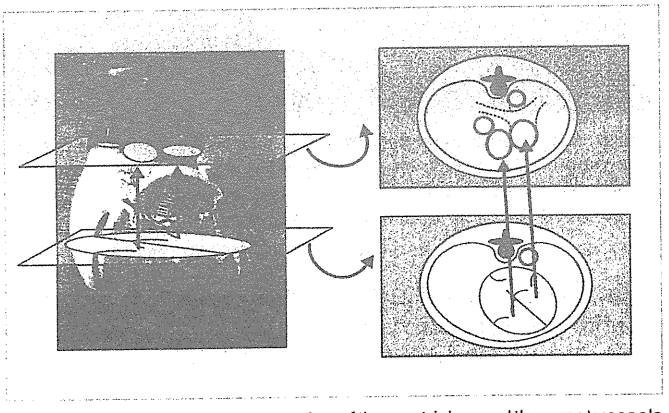

Fig. 13: Abnormal parallel connection of the ventricles and the great vessels

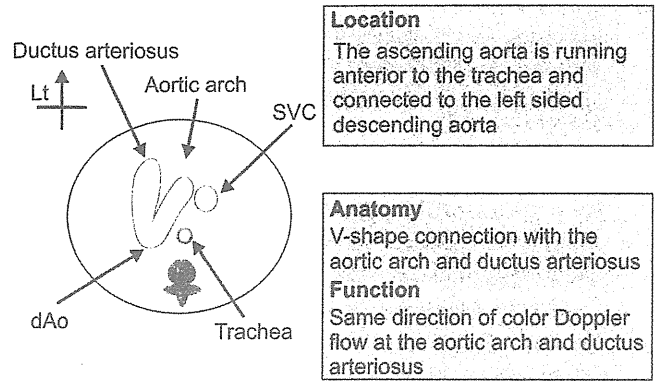

Fig. 14: Check list of the three-vessel and trachea view

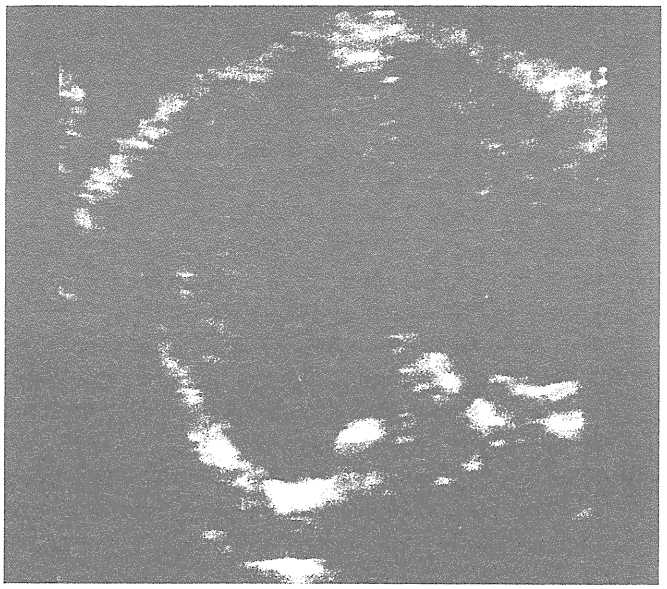

Fig. 15: A fetal echocardiographic image of three-vessel and trachea view

screening. This three-vessel and trachea view is useful for detecting variable vascular rings, which sometimes cause marked airway problems postnatally (Fig. 16).

For the location assessment, the aortic arch crosses anterior side of the trachea from right anterior to the left posterior, and connected to the descending aorta. There is no 'size' assessment in this view. For the detail anatomy assessment, the ascending aorta is connected to the descending aorta via the aortic arch and isthmus, and the aortic arch and the ductus arteriosus makes V shape at the left side of the trachea. For the function and blood flow assessment, the color Doppler flow reveals the flow to the same direction at both the ascending aorta and the ductus arteriosus.

ROLE OF THREE-DIMENSIONAL ECHOCARDIOGRAPHY TO THE SCREENING

Three-dimensional (3D) echocardiography may have important role for the both the basic and advanced screening of abnormal fetal heart.[9,10] The information of the side of the heart is already included to the 3D data, and the four simple transverse views for screening can be obtained from the 3D data set (Fig. 17). For the conventional two-dimensional echocardiography, fetal movement and limited window due to the fetal position often makes it difficult to do fetal heart screening. Whereas in the 3D echocardiography, any optimal screening image can be obtained without fetal movement once the 3D data set of the fetal heart is acquired and saved into the hard disk.

For only the basic screening, still 3D data set is sufficient to assess the location and the size using the four-chamber view and the three-vessel view (Fig. 18). For the advanced screening, STIC method is needed to assess the detail anatomy and the function and blood flow. The STIC method, 3D images with heart beat, can be created by automatic calculation of fetal heart rate from the acquired data set.

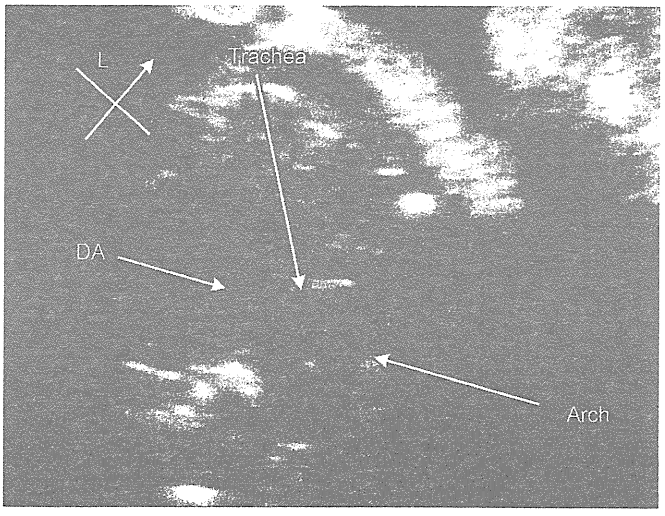

Fig. 16: A three-vessel and trachea view of the fetus with vascular ring caused by right sided aortic arch. The aortic arch is running right side of the trachea, and the ductus arteriosus (DA) is running left side of the trachea which making vascular ring

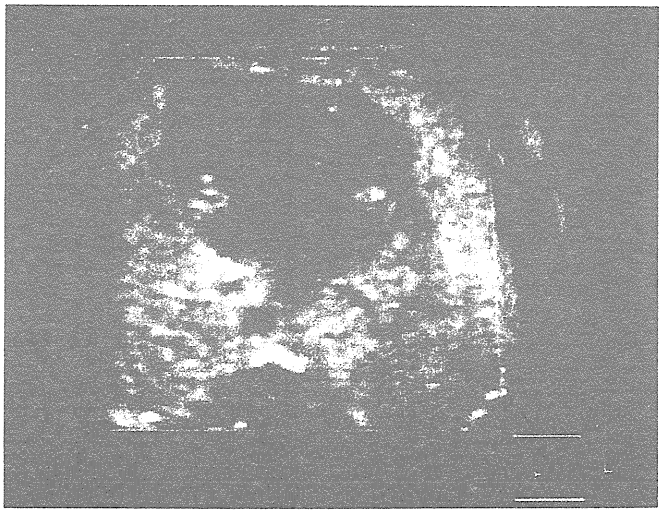

Fig. 17: Three-dimensional echocardiography in a case with common atrioventricular valve (asplenic syndrome). Optimal 2D cutting plane can be created from the 3D data set and demonstrated from optimal angle

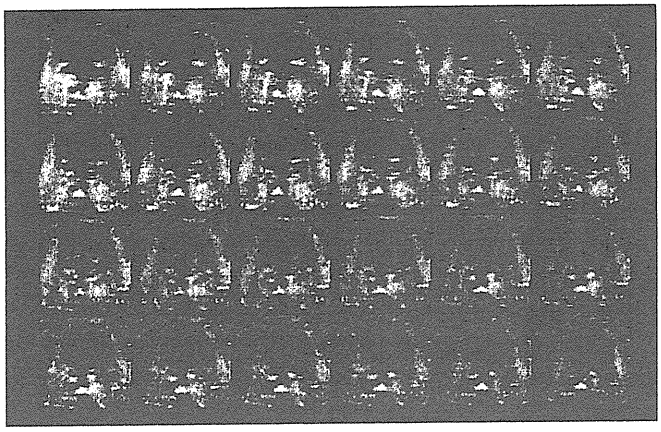

Fig. 18: Three-dimensional echocardiography in a case with common atrioventricular valve. Multiple parallel cutting planes obtained from 3D data set demonstrate the connection from the cardiac chambers to the vessels

CONCLUSIONS

Since the recent development of the fetal echocardiography and development of the perinatal management, the issue of the prenatal diagnosis of the fetal CHD is the screening system. In order to start fetal cardiac screening system in certain region, where the screeners are not familiar to the screening of CHD, step by step screening methods for taking account for the level of screener in certain area is needed. We present the fetal cardiac screening divided into two methods accounting for steps for learning screening technique; the basic screening and the advanced screening. The basic screening using only four-chamber view and three-vessel view with the assessment of location and size does not require complex knowledge of cardiac structures. Using this basic screening method, we believe more region start the systematic fetal screening program, and more fetuses have benefit for recent advanced perinatal management of CHD.

REFERENCES

1. Copel JA, Pilu G, Green J, Hobbins JC, Kleinman CS. Fetal echocardiographic screening for congenital heart disease: The importance of the four-chamber view. Am J Obstet Gynecol 1987;157:648-55.
2. Allan LD, Sharland GK, Milburn A, et al. Prospective diagnosis of 1,006 consecutive cases of congenital heart disease in the fetus. J Am Coll Cardiol 1994;23:1452-58.
3. Buskens E, Grobbee DE, Frohn-Mulder IME, et al. Efficacy of routine fetal ultrasound screening for congenital heart disease in normal pregnancy. Circulation 1996;94:67-72.
4. Bonnet D, Coltri A, Butera G, et al. Detection of transposition of the great arteries in fetuses reduces neonatal morbidity and mortality. Circulation 1999;99:916-18.
5. Carvalho JS, Mavrides E, Shinebourne EA, Campbell S, Thilaganathan B. Improving the effectiveness of routine prenatal screening for major congenital heart defects. Heart 2002;88: 387-91.
6. Cordes TM. Distinguishing right from left: A standardized technique for fetal echocardiography. J Am Soc Echo 1994;7:47.
7. Yoo S, Lee Y, Kim E, et al. Three-vessel view of the fetal upper mediastinum: An easy means of detecting abnormalities of the ventricular outow tracts and great arteries during obstetric screening. Ultrasound Obstet Gynecol 1997;9:173-82.
8. Yagel S, Arbel R, Anteby EY, Raveh D, Achiron R. The three vessels and trachea view (3VT) in fetal cardiac scanning. Ultrasound Obstet Gynecol 2002;20:340-45.
9. Devore GR, Polanco B, Sklansky MS, Platt LD. The 'spin' technique: A new method for examinination of the fetal outflow tracts using three-dimensional ultrasound. Ultrasound Obstet Gynecol 2004;24:72-82.
10. Herberg U, Steinweg B, Berg C, Breuer J. Echocardiography in the fetus: A systematic comparative analysis of standard cardiac views with 2D, 3D reconstructive and 3D real-time echocardiography. Ultrasound Obstet Gynecol 2010 (Epub ahead).

産婦人科の実際　第60巻 第6号　(2011年6月1日 発行)

産婦人科の実際

新生児ループス（心ブロック）を発症した抗SS-A抗体陽性妊婦の検討

穴見　愛　　福嶋恒太郎　　湯元康夫　　和氣徳夫

金原出版株式会社

臨床経験

新生児ループス（心ブロック）を発症した抗 SS-A 抗体陽性妊婦の検討

穴見　愛[*1]　福嶋恒太郎[*2]　湯元康夫[*2]　和氣徳夫[*3]

抗 SS-A 抗体による新生児ループス（特に心ブロック）は児に不可逆的な障害を残す可能性が高いことから，臨床現場から診療指針の作成が望まれてきた。抗 SS-A 抗体陽性妊婦は年間 1 万例と推測されるが，その児に心ブロックが発症する確率は 1%と稀であるため，単施設での経験に基づく研究は難しいのが現状であった。今回，母体ならびに胎児の管理に関する指針を導き出すことを目的として発足した多施設，多診療科から構成される研究班により行われた調査をもとに，産科的視点から検討を加えた。

はじめに

自己抗体のなかには母体から胎児へ移行して児に重大な疾患を招来するものがある。抗 SS-A 抗体は全身性エリテマトーデスやシェーグレン症候群患者が保有しているばかりでなく，無症候女性の 1%が本抗体を保有することから，1 年に 1 万人の抗 SS-A 抗体陽性者が出産することになる。抗 SS-A 抗体陽性母体の 1%前後に心ブロック児が出生する[3]といわれており，心ブロック児出生推定数はおよそ 100 例と稀であるため単施設での経験に基づく研究は不可能であった。また心筋炎を伴う場合には長じて心筋症につながる可能性があり胎児診断・治療方法を確立する必要性が指摘されていたが，多診療科の境界領域にある疾患であったことも相まって手つかずとなっている現状があった。このような経緯を経て，平成 21 年度厚生労働科学研究費補助金難治性疾患克服研究事業（「胎児・新生児障害の原因となる自己抗体陽性女性の妊娠管理指針の作成」研究班）が発足した。本研究は，児に不可逆的な障害を残す可能性の高い抗 SS-A 抗体による新生児ループス（特に心ブロック）を対象とし，症例の多い施設の内科医，産科医，小児科医が共同で研究し，母体ならびに胎児の管理に関する指針を導き出すことを目的としている。

新生児ループス（neonatal lupus erythematosus；NLE）は，新生児にみられる先天性心ブロックまたは亜急性皮膚ループス様皮疹を主症状とする症候群である。NLE ではそのほとんどの症例において母体の血清で抗 SS-A 抗体が陽性であることから，抗 SS-A 抗体が経胎盤的に胎児に移行することより発症すると考えられている。NLE の症状の多くは一過性で，母体から移行した抗体の消失に伴って生後 6 カ月以内に消失するが，完全房室ブロック（complete atrioventricular block；CAVB）が発症すると不可

＊1　Ai Anami　九州大学病院産科婦人科
＊2　Kotaro Fukushima, Yasuo Yumoto　九州大学病院総合周産期母子医療センター
＊3　Norio Wake　九州大学大学院医学研究院生殖病態生理学

逆性であり，60%以上の児で永久的にペースメーカーを必要とする。胎児にCAVBが出現する時期は妊娠18～24週の間とされ，この時期に胎児超音波検査を繰り返し行い早期発見に努めることが必要である。一部の症例では発症の過程でⅠ，Ⅱ度房室ブロックからⅢ度房室ブロック（CAVB）に移行するといわれている。

近年，BuyonらはNLEを出産するリスクのある妊婦の管理指針として，胎児エコーによるPR間隔の測定を妊娠中に定期的に行うことによって，房室ブロックを可逆的な段階（Ⅰ，Ⅱ度房室ブロック）で早期に発見し，PR間隔の延長が認められる症例に関しては経母体的に胎盤移行性のあるステロイド（デキサメサゾン）を投与することによってこれを治療し，CAVBの発症を予防する方法を提案している〔The PR Interval and Dexamethasone Evaluation (PRIDE) Prospective Study〕[5]（図1）。この管理指針に関してはいったん発症した症例に対するデキサメサゾンの経母体的投与の胎児への有効性，逆に言えば可逆的な段階での房室ブロックの指摘の精度が課題として挙げられる。PR間隔の測定を定期的に行うことは，患者にも医師にも負担が大きい点も課題である。

一方CAVBの予防方法として経母体的にステロイドを投与する方法も報告されている[2]。ステロイド投与の対象は，CAVB児出産の既往があり，抗SS-A抗体が陽性の場合を原則とし，妊娠12週からベタメタゾン2 mgを処方，20週から2週間ごとに半減する方法である。しかしステロイドの長期投与により中枢神経系への弊害をもたらす可能性もあり，慎重に検討されなければならない[6]。

しかしながら，抗SS-A抗体陽性妊婦のなかで，どのような症例がNLE（CAVB）を発症するリスクが高いかについてはJaeggiら[1]やLlanosら[4]の報告があるものの，現在まで一定の見解が得られておらず，上述のBuyonら，Brucatoらの治療的，予防的プロトコールのどちらにせよ，よりリスクの高い症例を選別することは重要な課題である。

本稿では，本研究に参加している4施設（国立成育医療研究センター，順天堂大学病院，筑波大学病院，九州大学病院）における抗SS-A抗体陽性妊婦例118症例を対象とし，どのような母体からNLE(CAVB)が発症するか，CAVBの診断・治療はどのように行われているかについて行われた調査において，産科的視点から検討を加えた結果を紹介する。

1．方　法

対象は4施設（国立成育医療研究センター，順天堂大学病院，筑波大学病院，九州大学病院）における抗SS-A抗体陽性妊婦例118症例とした。

118症例の抗SS-A抗体陽性妊娠例を抗SS-A抗体陽性の判明の契機，ならびに母体原疾患に対する治療の有無により7群（A～G群）に分類した（表1）。

母体の抗体価，胎児CAVB予防目的のステロイド投与の有無，胎児CAVBの発生率，発症した胎児CAVBに対する胎内治療の有無について検討を行った。統計学的検定は，χ^2検定を用いて行った。なお，本研究は，各施設の倫理委員会ならびに九州大学医系地区部局臨床研究倫理審査委員会の承認（承認番号21-71）を得て行った。

2．結　果

1 抗SS-A抗体陽性妊婦の背景と児罹病率

抗SS-A抗体陽性妊娠例118症例を抗SS-A抗体陽性の判明の契機，ならびに母体の原疾患に対する治療の有無により7群（A～G群）に分類し，その症例の内訳，NLE，CAVBの発症例数，CAVB発症率を表1に示す。

膠原病と診断されていた症例（A～D群）のうち，妊娠前から膠原病に対する治療を受けており，引き続き妊娠後も治療を受けていたものをA群とし，症例は43例あった。そのうちNLEを発症した症例を1例，胎児CAVBを発症した症例を6例認めた。A群でのCAVB発症率は14%（6/43）であった。同じく膠原病と診断されていた症例のうち，妊娠前は膠原病に対

妊婦における自己免疫疾患の評価(スクリーニング)

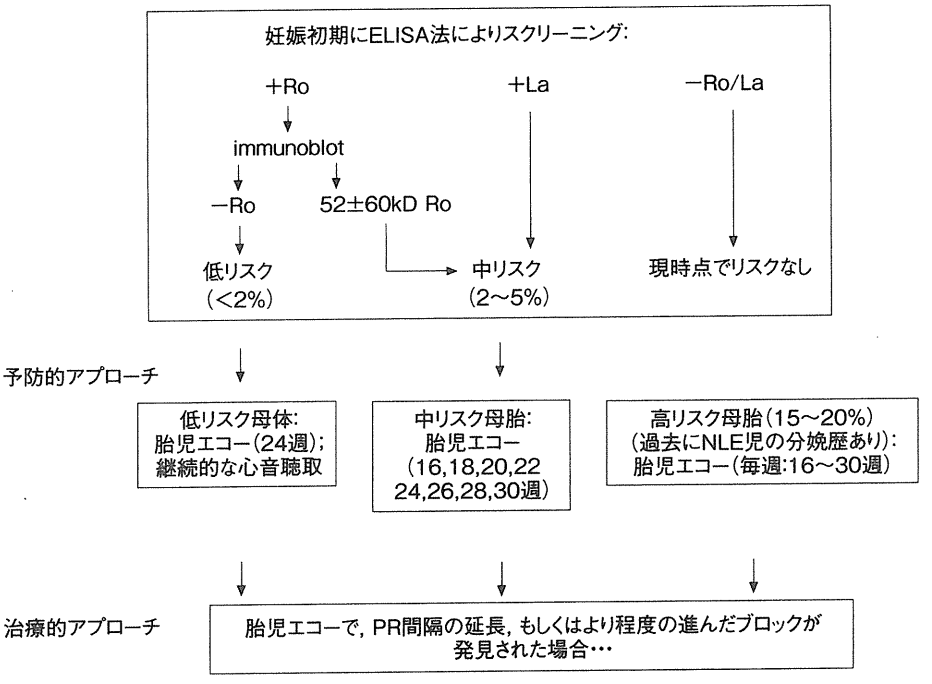

胎児期に心ブロックが発見された場合の
治療的アプローチ

状況	治療
1. 観察時の心ブロックの程度	
・Ⅲ度(発見から2週間以上経過)	・頻回にエコー評価(治療は行われない)
・Ⅲ度(発見から2週間以内)	・dexamethasone 4mg/日を6週間経口投与。Ⅱ度以下に改善した場合は分娩まで継続。
・Ⅱ度〜Ⅲ度の所見が交互に出現	・dexamethasone 4mg/日を分娩まで経口投与。Ⅲ度に進行するようなら6週間経口投与。
・Ⅱ度	
・PR間隔の延長(Ⅰ度)	
2. 心ブロックに心筋炎, 心不全徴候かつ/または胎児水腫を伴う	・dexamethasone 4mg/日を改善が認められるまで経口投与
3. 高度の胎児水腫	・dexamethasone 4mg/日経口投与に加え, 血漿交換により母胎血中抗体を除去する

NLE のリスクのある妊娠の管理指針

NLE 児の分娩歴を有する例を高リスク，52 kD の抗 SS-A/Ro 抗体と 48 kD の抗 SS-B/La 抗体を有する例を中リスク，60 kD の抗 SS-A/Ro 抗体を有する症例を低リスクと位置づけ，リスクの程度により胎児エコーで PR 間隔の測定を行う頻度を設定している。

(文献 5 より改変引用)

表1 抗 SS-A 抗体陽性妊婦の背景と胎児罹病率

群	診断契機	母体疾患への治療		症例数	既往妊娠 NLE/CAVB	現妊娠 NLE	現妊娠 CAVB	CAVB 発症率
		妊娠前	妊娠後					
A	膠原病	あり	あり	43	0	1	6	14%
B	膠原病	あり	—	4	0	0	1	25%
C	膠原病	—	—	39	1	3	2	5%
D	膠原病	—	あり	2	0	0	0	—
E	既往妊娠 NLE/CABV	—	—	5	5	0	0	—
F	現妊娠 CABV	—	—	10	0	0	10	100%
G	その他の妊娠合併症	2	6	15	0	0	0	—

抗 SS-A 抗体陽性妊婦 118 例を診断契機，ならびに治療状況により 7 群に分類し，児の罹病率を示した。
NLE：新生児ループス，CAVB：胎児心ブロック。

する治療を受けていたが妊娠判明後に治療を中止した症例を B 群とし，症例は 4 例であった。そのうち NLE 発症症例はなく，CABV を発症したのは 1 例で，発症率は 25%（1/4）であった。膠原病と診断された症例のうち妊娠前から膠原病に対する治療を受けておらず，妊娠判明後も治療が行われなかった症例を C 群とし，症例は 39 例あった。そのうち NLE 発症を 3 例，CAVB 発症を 2 例認めた。CAVB 発症率は 5%(2/39)であった。膠原病と診断されていた症例のうち妊娠前から妊娠判明後においても膠原病に対する治療を受けていなかった症例を D 群とし，症例は 2 例であった。この群では NLE，CAVB いずれの発症も認めなかった。膠原病とは関係なく，前回までの妊娠時で児に NLE または CAVB を認めたことから検索したところ母体が抗 SS-A 抗体陽性であることが判明した症例を E 群とし，症例は 5 例であった。このうち NLE，CAVB いずれも発症を認めなかった。今回の妊娠時に胎児に CAVB を発症したことから母体が抗 SS-A 抗体陽性であることが判明した症例を F 群とし，症例は 10 例であった。この群での CAVB 発症率は 100%となる。母体の習慣流産や身体所見，胎児に IUGR を認めたことなどから検索したところ母体が抗 SS-A 抗体陽性であることが判明した症例を G 群とし，症例は 15 例あった。そのうち NLE，CAVB 発症症例は認めなかった。

特に膠原病と診断されていた症例（A～D 群）において，妊娠前から膠原病に対して治療あり群（A，B 群）での CAVB 発症率は 15%（7/47），治療なし群（C，D）での発症率は 5%（2/41）であり，妊娠前から治療を受けていた群で発症率は高い傾向にあった。

2 抗 SS-A 抗体価と児の罹病

A～G 群の各群における抗 SS-A 抗体価（オクタロニー法）と CAVB ならびに NLE 発症との関係を図 2 に示す。膠原病と診断され妊娠前から治療を受けていた A 群においては抗体価が高いと罹患率が高くなる傾向があるが，今回の妊娠時に胎児が CAVB を指摘されたことを契機に抗 SS-A 抗体陽性が判明した F 群における抗体価は様々であり，少なくとも全症例を一群とした検討では，抗体価と児の罹患率に関しては明らかな関連は認めなかった。一方，抗体価 16 倍以下の症例では児に CAVB の発症は認め